

SHocks: structure, AcceleRation, dissiPation

Work Package 2
Structure of heliospheric shocks

Deliverable D2.1
Technical report on the low-Mach number shock
front structure

Michael Gedalin¹, Ephim Golbraikh¹, Christopher T. Russell²,
and Andrew P. Dimmock³

¹Department of Physics, Ben Gurion University of the Negev, Beer-Sheva, Israel

²Department of Earth, Planetary, and Space Sciences, University of California,
Los Angeles, California, USA

³Swedish Institute of Space Physics, Uppsala, Sweden

10/12/2021

This project has received funding from the European Union's Horizon 2020
research and innovation programme under grant agreement No 101004131



Document Change Record

Issue	Date	Author	Details
1.0	11.12.21	M. Gedalin	send to other co-authors for comments
1.1	19.12.21	M. Gedalin	final version

Table of Contents

1	Summary	3
2	Introduction	3
3	Data availability and quality	4
4	Results of analysis	5
5	Conclusions	5
6	References	6

1 Summary

Low-Mach number subcritical and supercritical shocks are expected to be almost planar and time-stationary, with only small deviations from this shape. Since the 1980s, theory of the low-Mach number shock structure gradually developed to a number of predictions regarding the relation of the basic features of the magnetic profile to the basic shock parameters, that is, the shock Mach number and the angle between the shock normal and the upstream magnetic field vector. Observations of low-Mach number shocks at other planets, as well as in the interplanetary plasma, allow to extend the comparison of theory with experiment. The WP2 Task 2.1 - Macroscopic structure of the low-Mach number shock front focused on the measurements of the magnetic field by Messenger at Mercury. The high temporal resolution of these measurements, 20 vectors/sec, allowed us to identify the features of the shock profile for a small selection of shocks, and to apply the theoretically predicted estimates to derive the Mach number and scales from the magnetic field data only. Application of the methods was later validated by similar analysis of a MMS observed shock and an independent analysis of the same shock with the conventional methods. A paper “Theory helps observations: Determination of the shock Mach number and scales from magnetic measurements” by M. Gedalin (BGU), E. Golbraikh (BGU), C. T. Russell (UCLA), and A. P. Dimmock (IRF), is being prepared for publication (the draft is attached).

2 Introduction

So far most of the detailed observational analyses of the shock structure have been done at the terrestrial bow shock [Greenstadt et al., 1980, Russell et al., 1982, Mellott and Greenstadt, 1984, Farris et al., 1993, Scudder et al., 1986, Bale et al., 2005, Krasnoselskikh et al., 2013]. Subcritical low-Mach number shocks have a monotonically increasing magnetic field profile of the ramp. Some of them have also an upstream coherent whistler wavetrain. At larger Mach numbers in supercritical shocks a foot, an overshoot, and downstream magnetic oscillations develop [Farris et al., 1993, Bale et al., 2005]. One of the central problems of the shock physics is the observational determination of the scales of these features: the ramp width, the wavelength of the whistler precursor, the foot width, and the distance between the maxima/minima of the downstream magnetic oscillations. This task requires first determination of the Mach number. At the Earth bow shock the most successful are the model normal and the mixed coplanarity normal [Gedalin et al., 2021]. The first one is based on the good knowledge of the global shock shape, the second one exploits the velocity measurements. If multi-spacecraft simultaneous measurements are available the relative timing of the shock crossing is often successful. Next step is the determination of the shock-spacecraft closing speed and the Mach number which requires good density measurements. Most spacecraft are not built well for the task of resolving the narrow solar wind beam, and often the upstream density is taken from measurements by other spacecraft at the Earth orbit. For interplanetary shocks or other planetary bow shocks such usage is not possible, and models of the global shock shapes are not developed to the same confidence level as for the Earth bow shock. At the same time, theoretical developments during the several decades of the shock studies resulted in

estimates of several scale parameters of the shock. The whistler precursor wavelength is evaluated in the reasonable assumption that the whistler stands in the shock frame [Krasnoselskikh et al., 2013]. The foot width is estimated from the reflected ion dynamics [Gosling and Thomsen, 1985, Gedalin, 1996a]. The distance between two successive maxima of downstream oscillations is estimated from the gyration of the downstream ion distributions [Gedalin et al., 2015, Gedalin, 2015, 2019]. The relation of the noncoplanar component of the magnetic field to the slope of the main magnetic field inside the ramp is established using two fluid hydrodynamics [Jones and Ellison, 1987, Gosling et al., 1988, Gedalin, 1996b, Newbury et al., 1997]. The expressions for the estimates are given in the attached paper draft. These estimates open a new possibility to compare theory with observations by cross-examination of various estimates using only the magnetic field measurements and by deriving the shock parameters from such examination. The Earth bow shock is typically a high-Mach number shock, so that it is desirable to exploit observations at other sites. Interplanetary shocks are typically low-Mach number shocks but, because of the high shock-spacecraft closing velocities, the resolution of the magnetic field profile is not sufficient for the analysis. The bow shocks at Venus and Mercury are better suited for the task. Among these, the Messenger observed Mercury bow shock is much less studied, while the temporal resolution there is good. This study focused on the Messenger shocks.

3 Data availability and quality

Messenger supplied shock magnetic field data during 2011-2014. Most of the data has temporal resolution of 20 samples/sec. Some data is of lower resolution of 10 samples/sec. The lower resolution data is not sufficient for the above described analysis. Availability of particle data is not sufficient for the study. The data reside on the website <https://pds-ppi.igpp.ucla.edu/mission/MESSENGER/MESS/MAG>. For each day the file with the corresponding magnetic field measurements was downloaded and each shock crossing was identified manually, according to the magnetic field jump. Such an identification may fail. A magnetic field jump in a shock must be accompanied by a density jump and a sharp velocity change (drop in the shock frame). Since the particle data are typically not available, some magnetic field jumps, which are not shocks, may be mistakenly identified as shocks. On the other hand, very noisy or quasi-parallel shocks may be easily missed. Figure 1 shows an example of the shock identification. From top to bottom : ± 20 s around the shock, ± 3 min around the shock, ± 2 hours around the shock, the whole day. The vertical red line shows the approximate position of the shock. The horizontal blue line at the bottom panel in fact consists of tightly packed blue points. The "blue line" at the panel shows that the temporal resolution is 20 samples/sec. Occasionally the resolution becomes 10 samples/sec. The objective of the manual shock search was not to properly identify all shocks. Instead, we wanted to identify a substantial number (hopefully most) shock candidates and make a gallery of the above 4-panel figures accessible for researchers. Many Messenger shocks are very noisy and moving. There are days which show many multiple shock crossings. Not all shocks are low-Mach number shocks. Some of the candidates look as high-Mach number shocks with multiple ramps. This issue

is probably worth separate investigation but is beyond the scope of Task 2.1. For the analysis we had to carefully select shocks which would have sufficient number of clearly identifiable features to allow cross-examination using the described estimates. Since Mach numbers are not known at the time of selection, the shocks with $B_d/B_u < 3$ were considered as plausible candidates.

4 Results of analysis

For the detailed analysis two low-Mach number shocks were selected. The first selected shock crossing occurred in the year 2011 on the day of year 083 at 12:25:00. It is a typical subcritical shock with B_d/B_u and a clean whistler precursor. For these measurements the shock normal can be determined only from the magnetic coplanarity. The shock was found to be quasi-perpendicular with $\theta_{Bn} = 67^\circ$. The two methods of the scale determination, a) using the whistler precursor wavelength and b) using the noncoplanar magnetic field inside the ramp, appeared to be in good agreement. Comparison with the estimates of the ramp width by Farris et al. [1993] gave the Mach number $M_A \approx 1.6$. In addition to the direct analysis of the magnetic profile, we applied the adjustable test particle analysis (ATPA) [Gedalin, 2016] which allows to numerically fit several parameters. The ATPA fitter Mach number was $M_A \approx 1.65$, in good agreement with the above estimate.

The second selected shock is a supercritical shock with a foot, overshoot, and undershoot. In this case estimating the whistler length from the noncoplanar magnetic field inside the ramp and, separately, the foot width, allows to immediately determine the Mach number as $M_A \approx 3.9$. Another estimate of the Mach number can be obtained from the approximate relation of the Mach number to the overshoot strength [Gedalin, 2021]. Taking the normalized NIF cross-shock potential $s = 2e\phi_{NIF}/m_p V_u^2 = 0.5$ gives the estimate $M_A \approx 4.1$. The agreement is within the precision of the determination of the shock angle and positions of various features.

Since the estimates made for Messenger shocks are made using only the magnetic field measurements, it would be desirable to verify the applied methods at a shock for which the conventional methods can be used. To this end we found a MMS observed low-Mach number shock which could be analyzed in both approaches (Figure 2). The Mach number found with the magnetic field data only was $M_A \approx 3.35$. The Mach number found using the magnetic field and particle data together was $M_A = 3.5$. Other details are given in the attached draft.

5 Conclusions

We have used the magnetic field data of Messenger to manually search and identify shock crossings. Two low-Mach number shocks were selected for a detailed analysis using the theoretically predicted estimates of the scales of various shock features. It is found that cross-examination of these estimates allows us to determine the Mach number of the shock and consistent evaluation of the shock structure components. The method was verified by applying the same approach to a MMS shock for which the conventional methods can be also used. The found good agreement allows us to conclude that our present theoretical understanding of the low-Mach number

shock structure successfully quantitatively describes the whistler precursor, the foot, the ramp, the overshoot, and the downstream magnetic oscillations. This completes the studies of the structure of the low-Mach number shocks and allows us to proceed to higher Mach numbers where deviations from planarity and time-dependence have to be taken into account.

6 References

- S D Bale, M A Balikhin, T S Horbury, V V Krasnoselskikh, H Kucharek, E Möbius, S N Walker, A Balogh, D Burgess, B Lembège, E A Lucek, M Scholer, S J Schwartz⁷ 10, and M F Thomsen. Quasi-perpendicular Shock Structure and Processes. *Space Science Reviews*, 118(1):161–203, June 2005. doi: 10.1007/s11214-005-3827-0.
- M Farris, C Russell, and M Thomsen. Magnetic structure of the low beta, quasi-perpendicular shock. *J. Geophys. Res.*, 98:15285–15294, 1993.
- M Gedalin. Ion reflection at the shock front revisited. *Journal of Geophysical Research*, 101(A):4871–4878, March 1996a. doi: 10.1029/95JA03669.
- M Gedalin. Noncoplanar magnetic field in the collisionless shock front. *Journal of Geophysical Research: Space Physics (1978–2012)*, 101(A5):11153–11156, May 1996b. doi: 10.1029/96JA00518.
- M Gedalin. Collisionless relaxation of non-gyrotropic downstream ion distributions: dependence on shock parameters. *J. Plasma Phys.*, 81:905810603, 2015. doi: 10.1017/S0022377815001154.
- M Gedalin. Transmitted, reflected, quasi-reflected, and multiply reflected ions in low-Mach number shocks. *J. Geophys. Res*, 121(1):10, 2016. doi: 10.1002/2016JA023395.
- M Gedalin, Y Friedman, and M Balikhin. Collisionless relaxation of downstream ion distributions in low-Mach number shocks. *Phys. Plasmas*, 22:072301, 2015. doi: 10.1063/1.4926452.
- Michael Gedalin. Kinematic Collisionless Relaxation of Ions in Supercritical Shocks. *Frontiers in Physics*, 7:692, August 2019. doi: 10.3389/fphy.2019.00114.
- Michael Gedalin. Shock Heating of Directly Transmitted Ions. *ASTROPHYSICAL JOURNAL*, 912(2):82, May 2021. doi: 10.3847/1538-4357/abf1e2.
- Michael Gedalin, Christopher T. Russell, and Andrew P. Dimmock. Shock Mach Number Estimates Using Incomplete Measurements. *J. Geophys. Res*, 126(10): e2021JA029519, 2021. ISSN 2169-9402. doi: 10.1029/2021JA029519.
- J T Gosling and M F Thomsen. Specularly reflected ions, shock foot thicknesses, and shock velocity determinations in space. *J. Geophys. Res*, 90:9893–9896, 1985. doi: 10.1029/JA090iA10p09893.

- J. T. Gosling, D. Winske, and M. F. Thomsen. Noncoplanar magnetic fields at collisionless shocks: A test of a new approach. *J. Geophys. Res.*, 93(A4):2735, 1988. ISSN 0148-0227. doi: 10.1029/JA093iA04p02735.
- E. W. Greenstadt, F. L. Scarf, C. T. Russell, J. T. Gosling, S. J. Bame, G. Paschmann, G. K. Parks, K. A. Anderson, R. R. Anderson, and D. A. Gurnett. A macroscopic profile of the typical quasi-perpendicular bow shock - Isee 1 and 2. *J. Geophys. Res.*, 85:2124–2130, 1980.
- Frank C. Jones and Donald C. Ellison. Noncoplanar magnetic fields, shock potentials, and ion deflection. *J. Geophys. Res.*, 92(A10):11205, 1987. ISSN 0148-0227. doi: 10.1029/JA092iA10p11205.
- V Krasnoselskikh, M Balikhin, S N Walker, S Schwartz, D Sundkvist, V Lobzin, M Gedalin, S D Bale, F Mozer, J Soucek, Y Hobara, and H Comişel. The Dynamic Quasiperpendicular Shock: Cluster Discoveries. *Space Science Reviews*, 178(2):535–598, October 2013. doi: 10.1007/s11214-013-9972-y.
- M M Mellott and E W Greenstadt. The structure of oblique subcritical bow shocks - ISEE 1 and 2 observations. *J. Geophys. Res.*, 89:2151–2161, 1984. doi: 10.1029/JA089iA04p02151.
- J A Newbury, C T Russell, and M Gedalin. The determination of shock ramp width using the noncoplanar magnetic field component. *Geophysical Research Letters*, 24(1):1975–1978, August 1997. doi: 10.1029/97GL01977.
- C Russell, M Hoppe, W Livesey, and J Gosling. Isee-1 and-2 observations of laminar bow shocks- velocity and thickness. *Geophys. Res. Lett.*, 9:1171, 1982.
- J D Scudder, T Aggson, T L Aggson, A Mangeney, C Lacombe, and C C Harvey. The resolved layer of a collisionless, high beta, supercritical, quasi-perpendicular shock wave. I - Rankine-Hugoniot geometry, currents, and stationarity. *J. Geophys. Res.*, 91(A10):11019–11052, 1986. doi: 10.1029/JA091iA10p11019.

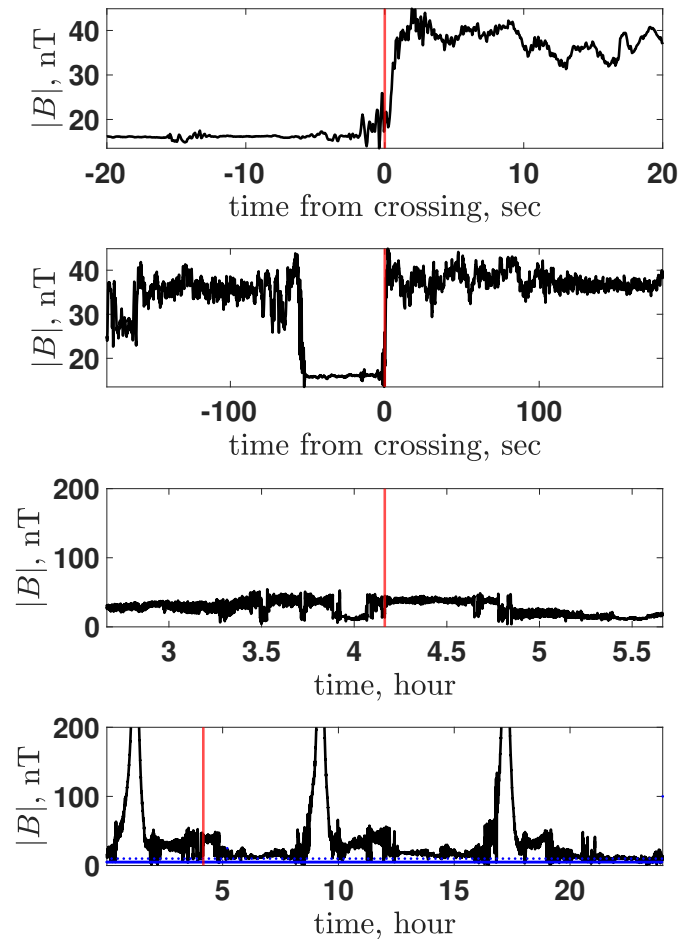


Figure 1: A shock candidate. From top to bottom: ± 20 s around the shock, ± 3 min around the shock, ± 2 hours around the shock, the whole day. The vertical red line shows the approximate position of the shock. The horizontal blue line at the bottom panel in fact consists of tightly packed blue points. The "blue line" at the panel shows that the temporal resolution is 20 samples/sec. Occasionally the resolution becomes 10 samples/sec.

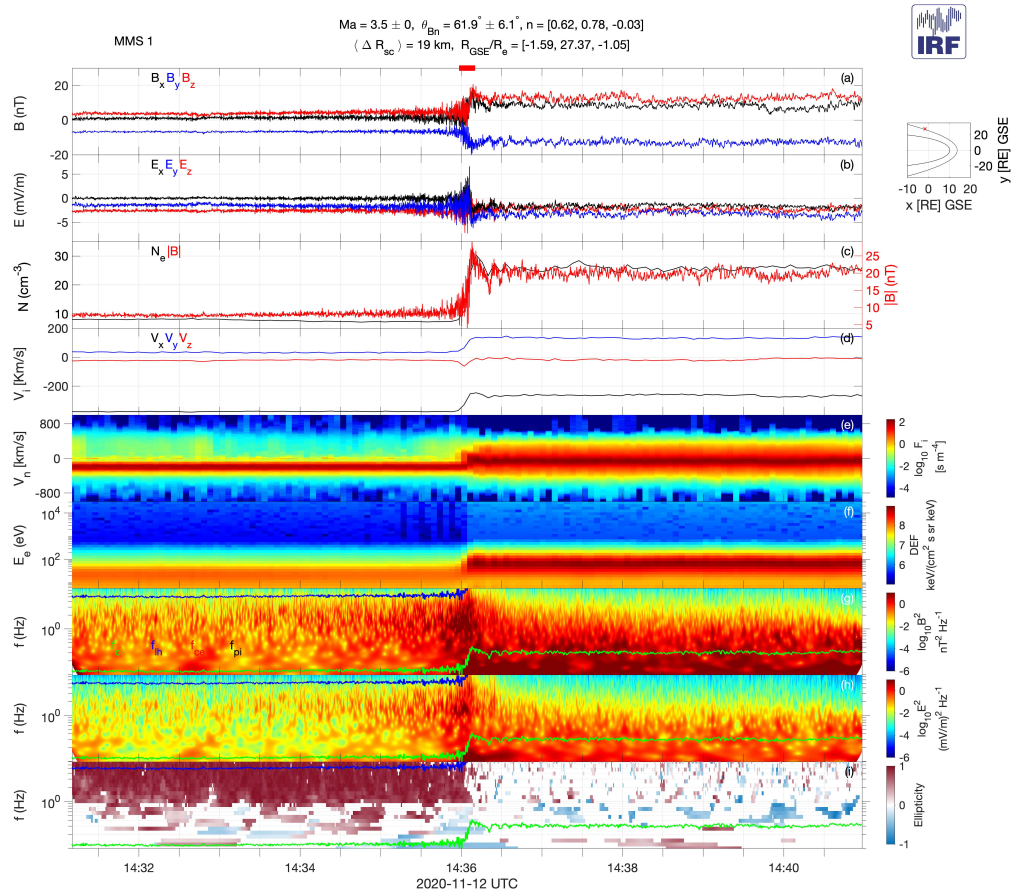


Figure 2: An overview of the MMS-1 observed shock used for verification.

Theory helps observations: Determination of the shock Mach number and scales from magnetic measurements

Michael Gedalin^{1,*}, Ephim Golbraikh¹, Christopher T. Russell², and Andrew P. Dimmock³

¹*Department of Physics, Ben Gurion University of the Negev, Beer-Sheva, Israel*

²*Department of Earth, Planetary, and Space Sciences, University of California, Los Angeles, California, USA*

³*Swedish Institute of Space Physics, Uppsala, Sweden*

Correspondence*:
Michael Gedalin
gedalin@bgu.ac.il

2 ABSTRACT

3 The Mach number is one of the key parameters of collisionless shocks. Understanding shock
4 physics requires also knowledge of the spatial scales in the shock transition layer. The standard
5 methods of the determination of the Mach number and the spatial scales require simultaneous
6 measurements of the magnetic field and the particle density, velocity, and temperature. While
7 magnetic field measurements are usually of high quality and resolution, particle measurements
8 are often either unavailable or not properly adjusted to the plasma conditions. We show that
9 theoretical arguments can be used to overcome the limitations of observations and determine the
10 Mach number and spatial scales of the low-Mach number shock when only magnetic field data
11 are available.

12 **Keywords:** collisionless shocks, magnetic field, planetary shocks, heliosphere,

1 INTRODUCTION

13 Collisionless shocks [1] are one of the most ubiquitous phenomena in space plasmas. The unfading
14 interest in collisionless shocks is related to the fact that they are the most efficient accelerators of charged
15 particles in the known universe [2–14]. A shock is a discontinuity in terms of magnetohydrodynamics
16 (MHD) [15], at which the flow velocity along the shock normal drops while the density increases. In
17 reality, this discontinuity has a finite width and the electric and magnetic field vary continuously inside
18 the transition from the upstream region of low density and entropy to the downstream region of higher
19 density and entropy. A collisionless shock efficiently converts the energy of the directed flow into the
20 thermal energy of charged particles, the energy of accelerated particles, and the field energy. The conversion
21 occurs via the interaction between charged particles and the electric and magnetic fields of the shock.
22 Thus, understanding the processes inside the shock requires, first and foremost, knowledge of the fields
23 inside the transition layer together with their dependence on time and space. Observational determination
24 of this is not an easy problem. Direct observational separation of spatial and temporal variations is not
25 possible with single-spacecraft measurements. Multi-spacecraft measurements help (see, e.g., Russell et al.
26 [16], Dunlop [17]) but to a limited extent. Determination of the Mach number and of the spatial scales

27 requires, in addition, sufficiently good particle measurements. At present, most spacecraft which study
 28 shocks, are not designed to properly measure parameters of narrow cold beams [18–22], and, therefore,
 29 the solar wind is not resolved to the required precision. At the same time, the available magnetic field
 30 measurements are typically very good. It would be helpful if the Mach number and the spatial scales
 31 could be reasonably estimated using magnetic field data alone. It makes sense to first attempt low-Mach
 32 number shocks which are expected to be nearly stationary and planar and have moderately structured
 33 profiles [23–31]. On the other hand, in a number of theoretical works dependences of several spatial scales
 34 on the Alfvénic Mach number have been derived and certain tools have been proposed for application to
 35 the magnetic field data [32–37]. The Mercury bow shock is typically a low-Mach number shock and the 20
 36 Hz MESSENGER magnetic field measurements are sufficiently good for the application of the proposed
 37 methods [38, 39]. In this paper, we demonstrate the efficiency and consistency of theoretical predictions by
 38 applying the proposed methods to selected shocks. The paper is organized as follows: first, we summarize
 39 the theoretical estimates of the width of various shock features proposed so far (section 2). Next, we briefly
 40 outline the numerical analysis used as an additional check (section 3). After that we analyze in detail two
 41 selected shock profiles.

2 THEORETICAL BASIS FOR ESTIMATES OF THE SHOCK SCALES AND MACH NUMBER

42 Several theoretical estimates are available for planar stationary shocks when ion reflection is weak. Note
 43 that these estimates allow to determination of the scales in terms of the ion inertial length but do not allow
 44 to determine the latter in dimensional units (km).

45 2.1 Phase-standing whistler precursor

46 In the shock with a coherent whistler precursor the wavelength of the whistler wave train can be estimated
 47 if the precursor is assumed to be phase standing in the shock frame [29, 36, 40, 41]:

$$\frac{\omega}{k} = c \frac{kc}{\omega_{pi}} \cos \theta_{Bn} = V_u \quad (1)$$

$$\lambda = \frac{2\pi}{k} = 2\pi l_W, \quad l_W = \frac{c \cos \theta_{Bn}}{M_A \omega_{pi}} \quad (2)$$

48 Conversion of the temporal scale into spatial scale then can be done by measuring the time between two
 49 successive maxima of the whistler precursor.

50 2.2 Foot length

51 Usually, the expression by Gosling and Thomsen [42] is used for estimation of the foot length. This
 52 expression is derived for a specularly reflected ion entering the shock with the velocity of the flow. More
 53 detailed studies have shown that ion reflection is non-specular and the foot length is substantially smaller
 54 and can be estimated as

$$L_{foot} \approx 0.5 \frac{V_u}{\Omega_u} = 0.5 M (c/\omega_{pi}) \quad (3)$$

55 where M is the Alfvénic Mach number [33].

56 2.3 Downstream magnetic oscillations

57 Coherent magnetic oscillations arise due the gyration of the ion distributions produced at the shock
 58 crossing [43–46]. If the oscillations are periodic this may indicate that the effect of the reflected ions is
 59 weak. For directly transmitted ions the distance between two successive maxima can be estimated as

$$\Delta = V_{drift} \frac{2\pi}{\Omega_d} = \frac{2\pi V_u}{\Omega_u} \left(\frac{B_u}{B_d} \right)^2 \quad (4)$$

60 The amplitude of the oscillations decreases due to the gyrophase mixing. The decay is faster for higher
 61 upstream ion temperatures. If the effect of reflected ions is significant, there may exist addition peaks/dips
 62 between the main maxima/minima [47]. In this case Δ would correspond to the distance between a
 63 maximum and the next second maximum, or approximately to the twice distance between two adjacent
 64 maxima.

65 2.4 Distance from the overshoot maximum to the undershoot minimum

66 This distance is more difficult to evaluate. As a rough approximation it can be estimated as a gyroradius
 67 of the ion, which just crossed the ramp, in the downstream magnetic field. Within the narrow shock
 68 approximation [48, 49] the ion speed upon crossing the shock is

$$v_d = v_u \sqrt{1 - s}, \quad s = \frac{2e\phi_{NIF}}{m_i V_u^2} \quad (5)$$

69 where $e\phi_{NIF}$ is the cross-shock potential in the normal incidence frame. Therefore, a rough approximation
 70 for the distance from the overshoot maximum to the undershoot minimum would be

$$L_{max,min} \approx \frac{V_u}{\Omega_u} \left(\frac{B_u}{B_d} \right) \sqrt{1 - s} \quad (6)$$

71 This estimate is less reliable than the others since the gyration occurs in the inhomogeneous magnetic field
 72 between the ramp and the undershoot.

73 2.5 Noncoplanar magnetic field

74 In laminar shocks or in shocks with weak ion reflection the noncoplanar magnetic field component inside
 75 the ramp is approximately [34, 35]

$$B_y = l_W \frac{dB_z}{dx} = \frac{c \cos \theta_{Bn}}{M\omega_{pi}} \frac{dB_z}{dx} \quad (7)$$

76 This approximation is not valid behind the ramp where the ion distributions begin to gyrate as a whole.

3 BASICS OF NUMERICAL ANALYSIS

77 Further check of the estimates will be done using the adjustable test particle analysis [50, 51]. We trace
 78 ions in a model low-Mach number shock profile which is given by the following expressions:

$$\frac{B_z}{B_u \sin \theta_{Bn}} = \left(\frac{R_z + 1}{2} \right) + \left(\frac{R_z - 1}{2} \right) \tanh \left(\frac{x}{D} \right) \quad (8)$$

$$\frac{B_d}{B_u} = \sqrt{R_z^2 \sin^2 \theta_u + \cos^2 \theta_u} \quad (9)$$

79 The electrostatic field along the shock normal is modeled using $E_x \propto \frac{dB_x}{dx}$ and

$$- \int E_x dx = \phi_{NIF} \quad (10)$$

80 while the noncoplanar component of the magnetic field is taken from (7). An incident Maxwellian
 81 distribution of ions is traced across the shock, the total ion pressure is numerically determined as a function

82 of the coordinate x along the shock normal. The pressure is inserted in the pressure balance

$$p_{i,xx} + p_e + \frac{B^2}{8\pi} = p_{i,xx,u} + p_{e,u} + \frac{B_u^2}{8\pi} \quad (11)$$

83 Here $p_{i,xx}$ is the total pressure, that is, the sum of the dynamic and kinetic pressure. The equation (11)
 84 is used to numerically find the magnetic field which would be consistent with the pressure balance. The
 85 shock parameters M, s, D, β are varied until the magnetic field derived from (11) converges to the initial
 86 model magnetic field. For low-Mach number shocks magnetic oscillations of the derived field around the
 87 downstream value are small, so that their effect on the ion motion can be neglected.

4 SHOCK 2011/083/12:25:00

88 Figure 1 shows the shock crossing and the context. The three top panels show the magnetic field ± 20
 89 s, ± 180 s, and ± 1.5 h around the crossing. The bottom panels show the whole day. The blue line is
 90 in fact very tightly packed points. Each point is the time step between the measurements. The value is
 91 multiplied by 100 to make it visible in the figure. Most of points are at 0.05 s, but periodically the step
 92 jumps to 0.1 s. This is a good day, the magnetic field is measured at the highest resolution of Messenger,
 93 20 samples/s. Figure 2 shows the normalized magnetic field rotated into the shock coordinates: x is along
 94 the shock normal, y is the noncoplanarity direction. The red vertical lines mark the upstream region
 95 used for the calculation of the normal from the magnetic coplanarity, the blue vertical lines mark the
 96 downstream region. The black vertical line marks the crossing time. The fields are normalized on the
 97 upstream magnetic field magnitude which is calculated by averaging the magnetic field vector over the
 98 upstream region and computing the magnitude of the derived mean magnetic field. The main magnetic field,
 99 B_z , has a clear monotonic ramp, a whistler precursor, and a barely noticeable overshoot: $B_d/B_u = 1.7$
 100 and $\max |B|/B_u = 1.75$. The noncoplanar magnetic field exhibits fluctuations at the spatial scale of the
 101 ramp and of the whistler precursor. The normal component fluctuates inside the ramp. The spatial scales
 102 of these fluctuations are substantially smaller than the ramp width. We tend to interpret these deviations
 103 from planarity as a small scale rippling inside the ramp which propagates along the shock surface. The
 104 normal component of the magnetic field does not have fluctuations at the whistler spatial scale outside
 105 the ramp, which makes us conclude that the whistler propagates or phase stands along the normal. The
 106 angle between the shock normal and the upstream magnetic field is $\theta_{Bn} = 67^\circ$, $\cos \theta_{Bn} = 0.4$. Moderate
 107 changes of the upstream and downstream intervals did not affect the normal determination noticeably.
 108 Figure 3 is a closeup of Figure 2 but plotted using points to show explicitly the resolution of the magnetic
 109 field measurements. The magenta line is for the magnetic field magnitude. The horizontal black line marks
 110 $B = 0$. The magnetic field increase in the ramp is nearly linear, and the noncoplanar magnetic field has a
 111 rather broad maximum. The behavior is consistent with the relation. The magnetic field is measured as
 112 a function of time in the spacecraft frame. Accordingly, in what follows all scales are given as temporal
 113 equivalents of the corresponding spatial scales. Proper conversion of temporal durations into spatial lengths
 114 should be done by multiplying by the unknown shock speed V_{sh} in the spacecraft frame. This speed cannot
 115 be determined in dimensional units (km/s) without density measurements. The time separation of the
 116 two successive maxima of the whistler precursor is $\Delta t_W = 3.19$ s which gives the spatial-to-temporal
 117 correspondence $l_W = V_{sh} \cdot 0.5$ s. Using (7) one gets $l_W = V_{sh} \cdot 0.6$ s. The agreement is quite good. The
 118 ramp width is $D = V_{sh} \cdot 2.4$ s, that is,

$$D \approx 4 \frac{c \cos \theta_{Bn}}{M_A \omega_{pi}} \approx 1.6 \frac{c}{M_A \omega_{pi}} \quad (12)$$

119 Assuming $D \approx c/\omega_{pi}$ we get an estimate of the Alfvénic Mach number: $M_A \approx 1.6$.

120 The shock is laminar which indicates low β . Figure 4 shows the results of the adjustable test particle
 121 analysis. The shock angle and width were taken from the above estimates, while the Mach number M , the
 122 cross-shock potential s , and the ion β_i were varied. The best convergence to the downstream magnetic field
 123 was found for $M = 1.65$, $\beta_i = 0.1$, and $s = 0.63$. The overshoot in the derived profile is also in agreement
 124 with the observations.

5 SHOCK 2013/047/06:57:00

125 Figure 5 shows the shock crossing and the context, similarly to Figure 1. Figure 6 shows the normalized
 126 magnetic field rotated into the shock coordinates, similarly to Figure 2. This shock has a clear overshoot.
 127 The downstream-to-upstream main magnetic field ratio is $R_d = B_d/B_u = 2.66$ and $\max |B|/B_u = 3.54$.
 128 The angle between the shock normal and the upstream magnetic field is $\theta_{Bn} \approx 63^\circ$, $\cos \theta_{Bn} \approx 0.45$.
 129 Moderate changes of the upstream and downstream intervals did not affect the normal determination
 130 noticeably. There is high-frequency turbulence present. We remove it using the wavelet denoising as
 131 follows: a) 2^{11} points of data are taken around the crossing time to cover sufficiently the upstream and
 132 downstream regions, b) the Daubechies-10 wavelet transform is applied, c) 5 smallest scales are removed,
 133 and d) the inverse wavelet transform is performed. The procedure is done for B_x, B_y, B_z and separately
 134 for $|B|$, since otherwise the foot region is smeared out. Figure 7 shows the magnetic field magnitude with
 135 the high-frequency noise removed. The maximum magnetic field is now $R_m = |B_{dn,max}|/B_u = 3.3$. We
 136 shall adopt this value as the maximum overshoot magnetic field. Figure 8 shows some meaningful points
 137 marked at the magnetic field profile. Among these the most important for us will be the beginning of the
 138 foot at $t_1 = -10$ s, the end of the foot and the beginning of the ramp at $t_2 = -1.9$ s, with the elevation of
 139 the magnetic field of $\Delta B_{foot}/B_u = 0.1$, and the overshoot maximum at $t_3 = 0.7$ s, with the additional
 140 elevation of the magnetic field of $\Delta B_{ro}/B_u = 2.2$. The minimum of the undershoot occurs at $t_5 = 5.8$
 141 s, and the magnetic field there drops to $B_5/B_u = 2$, well below the downstream value. The width of the
 142 foot is estimated as $L_{foot} \approx 0.5M(c/\omega_{pi}) = V_{sh} \cdot 8.1$ s, where M is the Alfvénic Mach number [33].
 143 Figure 9 shows all three components of the magnetic field with high-frequency noise removed. The normal
 144 component B_x (red line) remains reasonably constant with only small variations inside the ramp. The
 145 noncoplanar component has the maximum value of $B_y/B_u \approx 0.4$ inside the ramp where the slope is the
 146 steepest, $(1/B_u) \frac{dB_z}{dt} \approx 0.84 \text{ s}^{-1}$, and $\frac{dB_z}{dx} = (1/V_{sh}) \frac{dB_z}{dt}$. This behavior implies that the relation (7) may
 147 be a good estimate [35]. Using it we get

$$L_W = \frac{c \cos \theta}{M \omega_{pi}} V_{sh} = V_{sh} \cdot 0.47 \text{ s} \quad (13)$$

148 Note that this relation is not valid behind the ramp because of the strong non-gyrotropy of the ion
 149 distribution [32]. Together with the estimate of L_{foot} we get the estimate of the Mach number

$$M = \sqrt{\frac{2L_{foot} \cos \theta}{L_W}} \approx 3.9 \quad (14)$$

150 Another estimate of the Mach number can be obtained from [49]

$$R_m^2 = 2M^2(1 - \sqrt{1 - s}) + 1 \quad (15)$$

151 where $s = 2e\phi_{NIF}/m_p V_u^2$ is the normalized NIF cross-shock potential. Taking $s = 0.5$ one gets $M \approx 4.1$.
 152 The two estimates agree very well. There should be no illusions though since all these are approximations.
 153 Using $M \approx 4$ we get

$$\frac{c}{\omega_{pi}} \approx V_{sh} \cdot 4 \text{ s}, \quad \frac{V_u}{\Omega_u} = M \left(\frac{c}{\omega_{pi}} \right) \approx V_{sh} \cdot 16 \text{ s} \quad (16)$$

154 The distance between the maximum of the overshoot and the minimum of the undershoot is 5 s. A rough
 155 estimate of this distance is

$$\frac{V_d}{\Omega_d} \approx \left(\frac{\sqrt{1-s}}{R_d} \right) \left(\frac{V_u}{\Omega_u} \right) \approx V_{sh} \cdot 4.25 \text{ s} \quad (17)$$

156 which is not bad at all. Consistence of all these estimates encourages to conclude that the chosen $s = 0.5$ is
 157 not far from reality.

158 Absence of downstream magnetic oscillations, that is, only one overshoot and undershoot, indicates
 159 high β . Figure 10 shows the results of the adjustable test particle analysis. The best convergence to the
 160 downstream magnetic field was found for $M = 4$, $\beta_i = 0.75$, and $s = 0.5$. The overshoot in the derived
 161 profile is also in agreement with the observations. The position of the undershoot is close to the predicted.
 162 However, the magnetic field in the undershoot of the derived profile is somewhat higher than the observed
 163 one, probably because the overshoot modifies the ion motion. The initial profile used for adjustment was
 164 a simple tanh-like profile. It is possible that using a more sophisticated model with an overshoot and
 165 undershoot a better agreement could be achieved. We leave this issue for further studies.

6 VERIFICATION

166 There are no particle data for Messenger. The above analysis has been done using the magnetic field
 167 measurements alone. It is desirable to verify this analysis with shocks for which the Mach number and
 168 the scales could be determined by the above methods and, independently, by the conventional methods
 169 involving additional measurements. For this task an MMS1 shock was selected with sufficient magnetic
 170 features to apply the above approach. Two independent analyses have been performed: one applied the
 171 theoretical estimates to the magnetic profile without utilizing any other information, the other one was
 172 done in the standard way. Below we present the comparison. The chock crossing occurred at 2020-11-12
 173 14:36:04. Figure 11 shows a part of the shock, $|\mathbf{B}|/B_u$, in GSE coordinates, with the time set to zero at
 174 the shock crossing. The black line shows the normalized magnetic field magnitude. The sampling rate
 175 is 16 measurements per second. The upstream magnetic field is determined by averaging over about 20
 176 first seconds of the figure. The downstream magnetic field is determined by averaging over about 50 last
 177 seconds of the figure. The shock normal is determined using magnetic coplanarity. The found shock normal
 178 is $\hat{n} = (0.6275, -0.7786, 0.0005)$. The red line shows the denoised magnetic field. The denoising, that is,
 179 removal of high frequency fluctuations in order to retain only what is assumed to be the stationary profile,
 180 is done applying discrete wavelet transform. The Wavelab850 procedure with the Daubechies 10 wavelet
 181 was applied to the 4096 point data and 5 finest scales were removed. The vertical blue lines show the
 182 chosen beginning and end of the foot used for further analysis. The duration of the foot is 10.16 s. The
 183 denoised magnetic field is used for the determination of $R_d \approx 2.5$ and $R_m \approx 3.6$. Figure 12 shows the
 184 noncoplanar and main magnetic field components in the vicinity of the ramp. Using (3) and (7) the Mach
 185 number is estimated as $M \approx 3.35$ and the ion inertial length corresponds to the duration ≈ 6.0 s. Using the
 186 distance between the two adjacent downstream maxima gives a result inconsistent with other estimates.
 187 Using the twice the distance together with the foot length also gives $M \approx 3.35$. Note that the precision of

188 the determination of the durations used for the estimates and the application of the wavelet transform are
189 not sufficient to ensure the above excellent agreement of the Mach number estimates.

The shock was independently analyzed using the MMS magnetic field and particle (density and velocity) measurements. The upstream and downstream magnetic field vectors in GSE coordinates are: $\mathbf{B}_u = (1.48, -6.53, 4.52)$ nT and $\mathbf{B}_d = (7.93, -12.94, 12.4)$ nT, respectively. The upstream and downstream velocity vectors in the spacecraft frame and GSE coordinates are $\mathbf{V}_1 = (-376, 33, -19)$ km/s and $\mathbf{V}_2 = (-264, 133, -18)$ km/s, respectively. The upstream and downstream number densities, measured by MMS, are $N_u = 8.11 \text{ cm}^{-3}$ and $N_d = 23.12 \text{ cm}^{-3}$, respectively. The model shock normal [52] $\hat{n} = (0.62, 0.78, -0.03)$ was used for the determination of the shock speed V_{sh} and the upstream velocity V_u :

$$V_{sh} = \frac{(N_d \mathbf{V}_2 - N_u \mathbf{V}_1) \cdot \hat{n}}{N_d - N_u}, \quad V_u = \frac{|(\mathbf{V}_2 - \mathbf{V}_1) \cdot \hat{n}|}{1 - N_u/N_d} \quad (18)$$

190 The Mach number is $M = V_u/V_A$, where $V_A^2 = B_u^2/4\pi N_u m_p$. The derived Mach number is $M = 3.68$
191 with the shock speed of $V_{sh} = 20.3$ km/s. Since the spacecraft instruments are not quite appropriate for
192 catching the cold solar wind, the OMNI density [53] is often used to replace the upstream ion density
193 measured by the spacecraft. In this case the OMNI density is $N_{u,OMNI} = 7.4 \text{ cm}^{-3}$, and the corresponding
194 Mach number is $M = 3.36$, with the shock speed of $V_{sh} = 10$ km/s. The Mach numbers obtained in
195 two approaches differ by less than 10%, which is within the precision of the determination of the shock
196 parameters.

7 DISCUSSION AND CONCLUSIONS

197 In this study we applied the theoretical estimates to the magnetic field measurements in order to determine
198 the Alfvénic Mach number and the scale parameters of two low-Mach number shocks. One of these shocks
199 has a very low overshoot and a clear whistler precursor. Another one possesses a substantial overshoot
200 and a foot. In both cases we were able to estimate the Mach number using at least two independent
201 theoretical approaches. In both cases we found good agreement between the various methods. In addition,
202 this allowed us to determine the correspondence of the duration of the measurement of a particular feature
203 to its physical spatial scale, in terms of the upstream convective gyroradius and/or ion inertial length. As
204 always, determination of the shock parameters requires making some assumptions, like stationarity and
205 planarity. Although at this stage the methods were applied to rather clean shocks with classical profiles,
206 they will possibly allow extension to less favorable cases, in part by comparison with the success of the
207 present study. The method has been tested with an MMS observed shock, for which sufficiently good
208 particle measurements are also available. The Mach number obtained with the magnetic measurements and
209 theory and the Mach number obtained with both magnetic field and particle measurements, differ by less
210 than 10%, which is encouraging.

CONFLICT OF INTEREST STATEMENT

211 The authors declare that the research was conducted in the absence of any commercial or financial
212 relationships that could be construed as a potential conflict of interest.

FUNDING

213 This research was partially supported by the European Union's Horizon 2020 research and innovation
214 programme under grant agreement No 101004131.

DATA AVAILABILITY STATEMENT

215 No new datasets were produced in this study.

FIGURE CAPTIONS

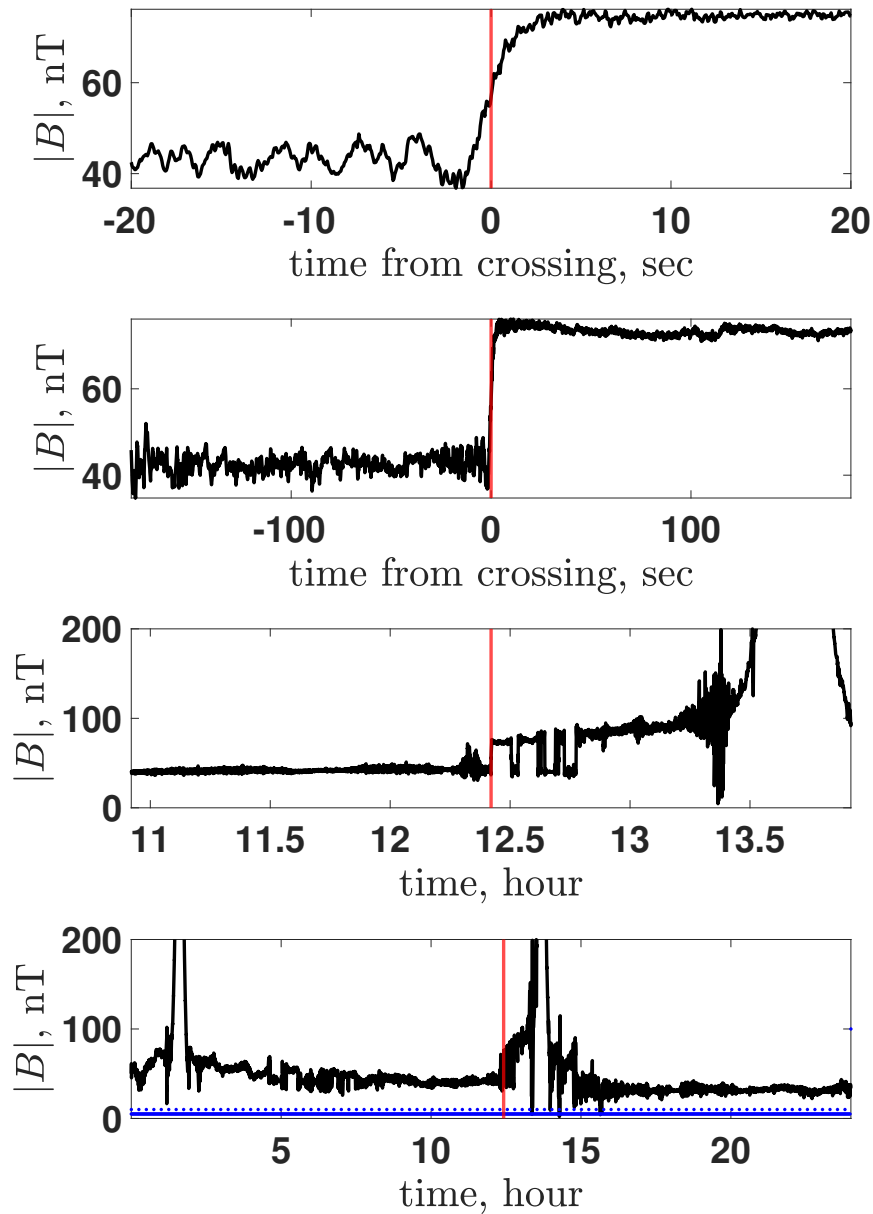


Figure 1. Magnetic field magnitude. Top 3: a) ± 20 s around the crossing, b) ± 180 s around the crossing, c) ± 1.5 h around the crossing. Bottom: the whole day, blue dots show the resolution 20 samples/s.

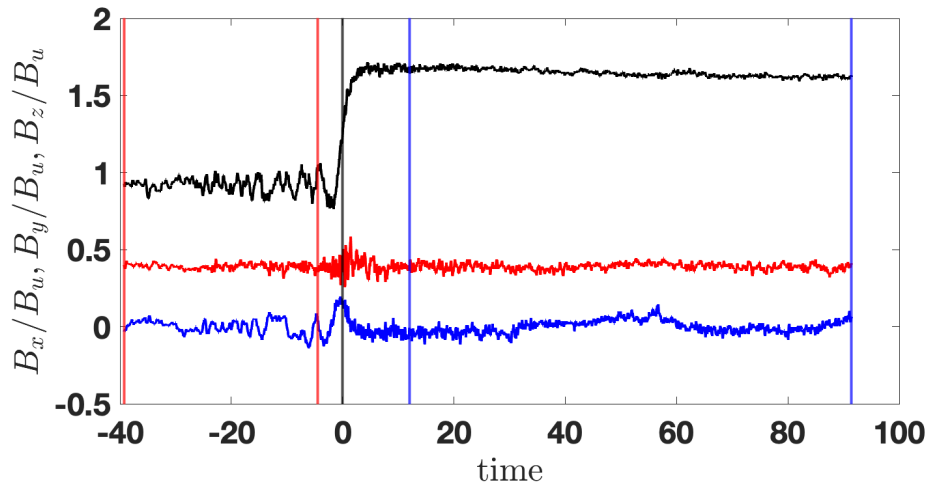


Figure 2. The normalized magnetic field rotated into the shock coordinates: x is along the shock normal, y is the noncoplanarity direction. The red vertical lines mark the upstream region used for the calculation the normal from magnetic coplanarity, the blue vertical lines mark the downstream region. The black vertical line marks the crossing time.

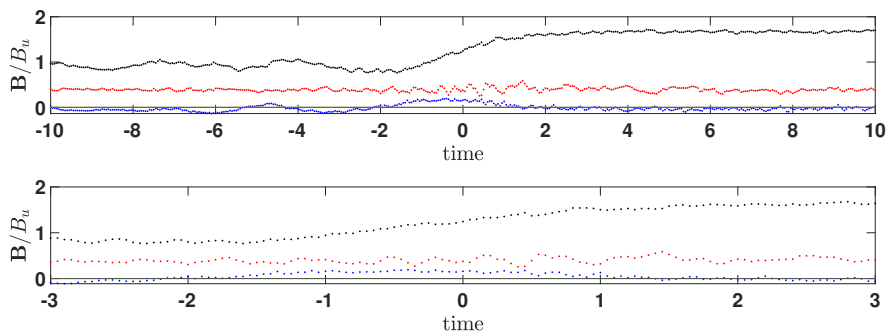


Figure 3. Closeup of Figure 2.

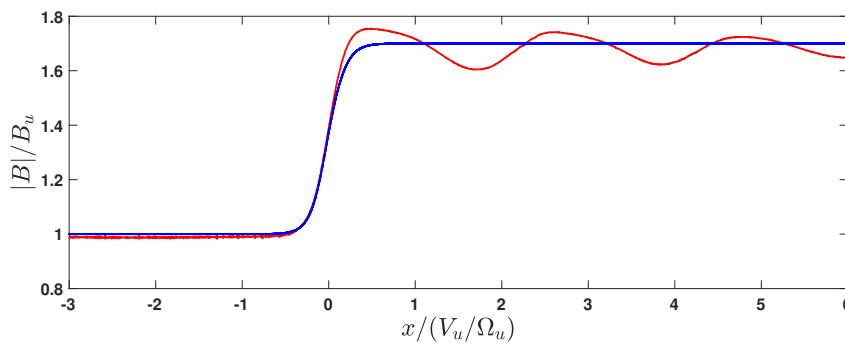


Figure 4. Profile adjusted using test particle analysis with $M = 1.65$, $\beta_i = 0.1$, and $s = 0.63$. The initial profile is shown by the blue line. The red line is the magnetic field derived from the pressure balance.

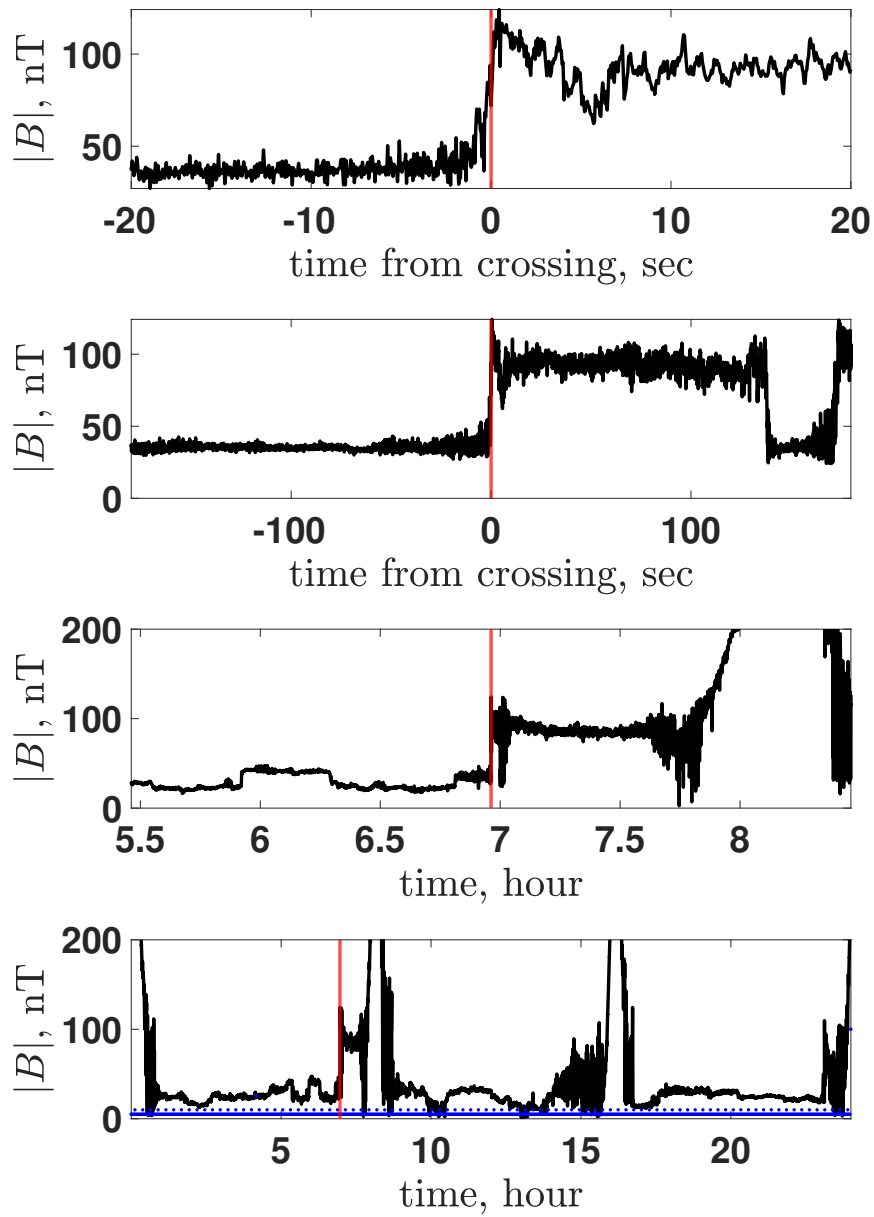


Figure 5. Magnetic field magnitude. Top 3: a) ± 20 s around the crossing, b) ± 180 s around the crossing, c) ± 1.5 h around the crossing. Bottom: the whole day, blue dots show the resolution 20 samples/s.

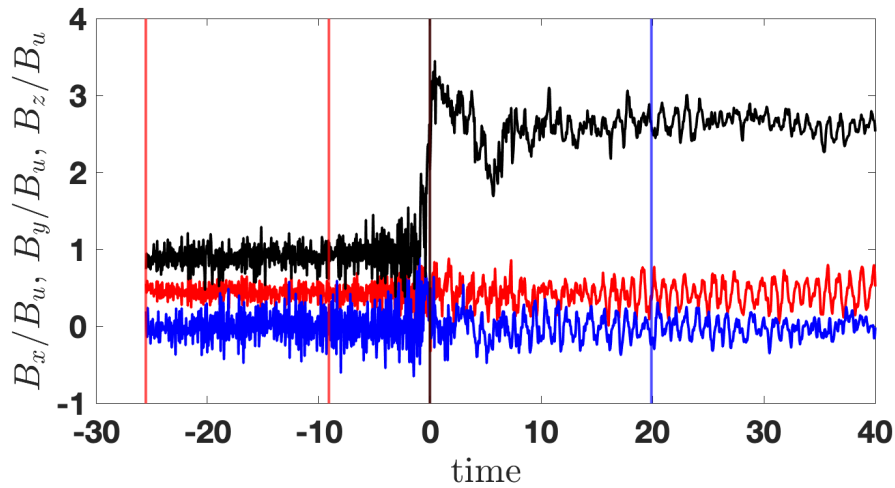


Figure 6. The normalized magnetic field rotated into the shock coordinates: x is along the shock normal, y is the noncoplanarity direction. The red vertical lines mark the upstream region used for the calculation the normal from magnetic coplanarity, the blue vertical lines mark the downstream region. The black vertical line marks the crossing time.

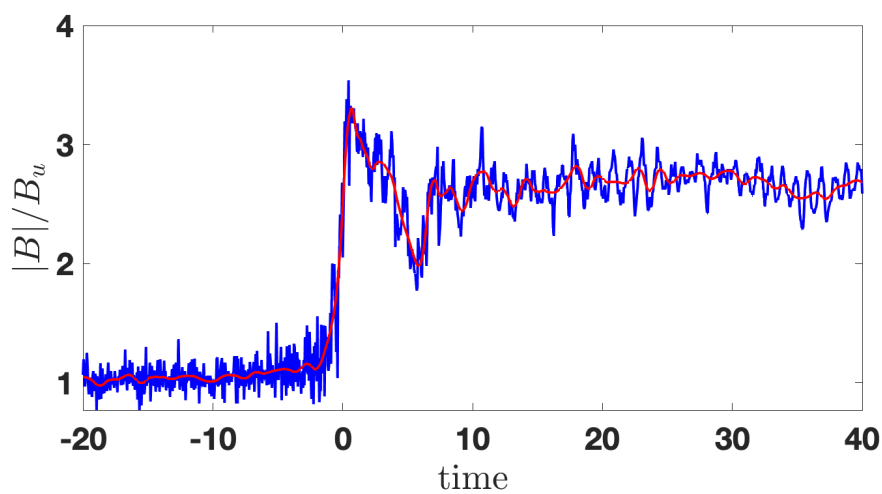


Figure 7. The original (blue) and the denoised (red) B .

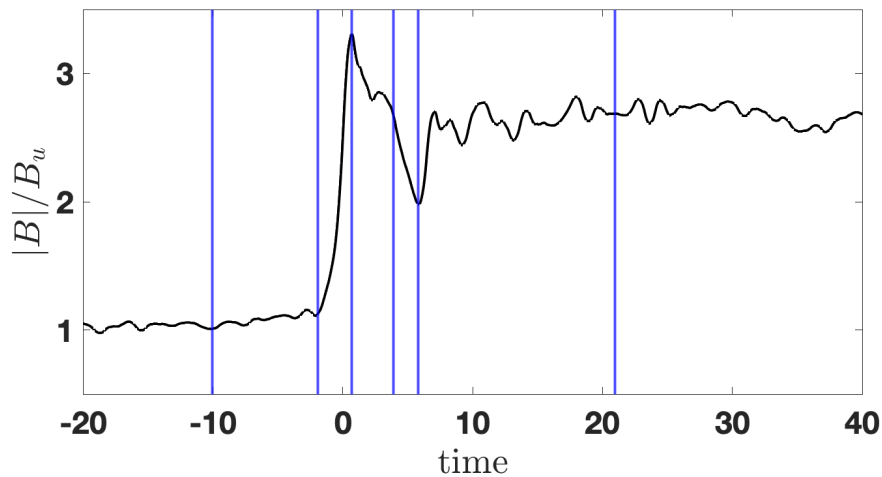


Figure 8. The denoised B and the meaningful points, from left to right: the beginning of the foot, the end of the foot and the beginning of the ramp, the overshoot maximum, the point where the magnetic field decreases to the value nearly equal to the downstream magnetic field magnitude, the minimum of the undershoot, the point where the mean magnetic field essentially levels off.

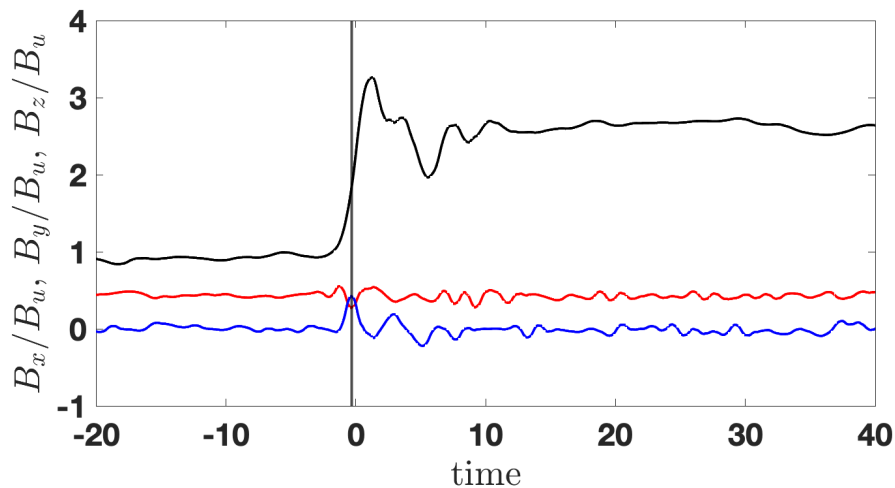


Figure 9. Three components of the denoised magnetic field: B_x (red), B_y (blue), and B_z (black). The maximum of B_y lies inside the ramp at the point with the steepest slope.

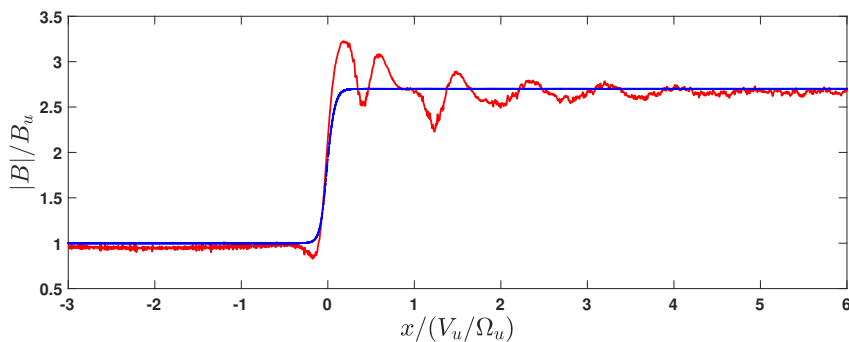


Figure 10. Profile adjusted using test particle analysis with $M = 4$, $\beta_i = 0.75$, and $s = 0.5$. The initial profile is shown by the blue line. The red line is the magnetic field derived from the pressure balance.

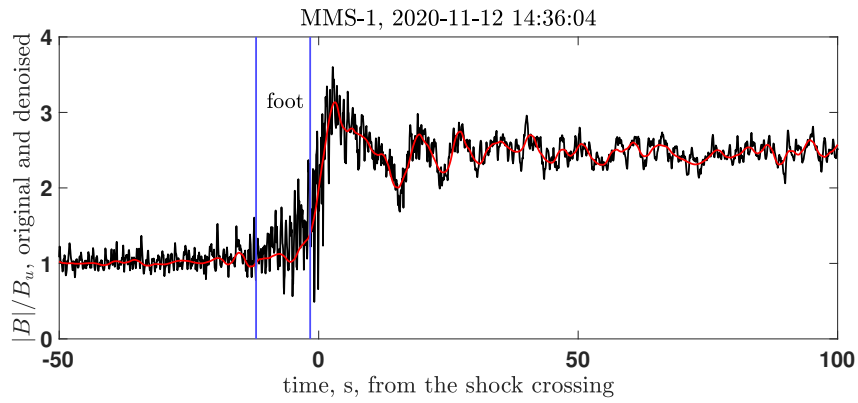


Figure 11. The MMS shock used for verification. The black line shows the normalized magnetic field magnitude. The red line shows the denoised magnetic field. The vertical blue lines show the beginning and the end of the foot. See details in text.

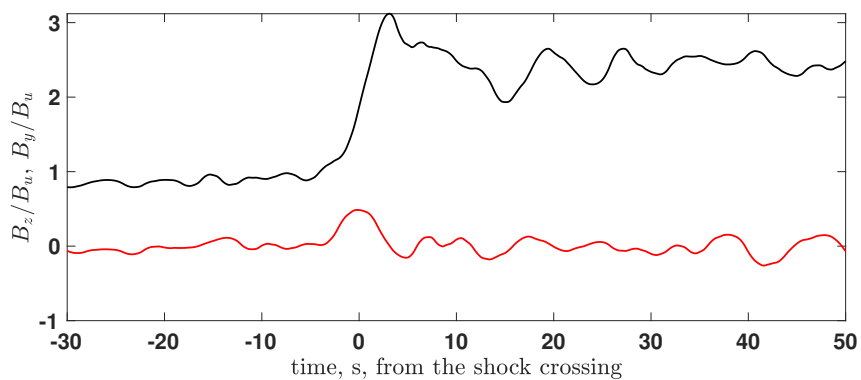


Figure 12. The noncoplanar magnetic field B_y and the main magnetic field component B_z .

REFERENCES

- 216 [1] Sagdeev RZ. Cooperative Phenomena and Shock Waves in Collisionless Plasmas. *Rev. Plasma Phys.*
217 **4** (1966) 23.
- 218 [2] Jokipii JR. Cosmic-Ray Propagation. I. Charged Particles in a Random Magnetic Field. *Astrophys. J.*
219 **146** (1966) 480–. doi:10.1086/148912.
- 220 [3] Roelof EC. Propagation of solar cosmic rays in the interplanetary magnetic field. ed H Ögelmann & J
221 R Wayland, editor, *Lectures in High Energy Astrophysics*, (NASA SP-199; Washington, DC: NASA
222 Scientific and Technical Information Division) (1969), 111.
- 223 [4] Axford WI, Leer E, Skadron G. The acceleration of cosmic rays by shock waves. *International*
224 *Cosmic Ray Conference, 15th, Plovdiv, Bulgaria, August 13-26, 1977, Conference Papers. Volume*
225 *11. (A79-44583 19-93) Sofia, B'lgarska Akademiia na Naukite, 1978, p. 132-137.* (Plovdiv) (1977),
226 13–26.
- 227 [5] Krymskii GF. A regular mechanism for the acceleration of charged particles on the front of a shock
228 wave. *Soviet Physics Doklady* **22** (1977) 327.
- 229 [6] Vasilev VN, Toptygin IN, Chirkov AG. Interaction between energetic particles and a shock front in a
230 turbulent medium. *Geomagnetism and Aeronomy* **18** (1978) 415–422.
- 231 [7] Bell AR. The acceleration of cosmic rays in shock fronts. I. *MNRAS* **182** (1978) 147–156.
- 232 [8] Blandford RD, Ostriker JP. Particle acceleration by astrophysical shocks. *Astrophys. J.* **221** (1978)
233 L29–L32. doi:10.1086/182658.
- 234 [9] Toptyghin IN. Acceleration of particles by shocks in a cosmic plasma. *Sp. Sci. Rev.* **26** (1980) 157–213.
235 doi:10.1007/BF00167370.
- 236 [10] Jokipii JR. Particle drift, diffusion, and acceleration at shocks. *Astrophys. J.* **255** (1982) 716–720.
237 doi:10.1086/159870.
- 238 [11] Drury LO. An introduction to the theory of diffusive shock acceleration of energetic particles in
239 tenuous plasmas. *Rep. Progr. Phys.* **46** (1983) 973–1027. doi:10.1088/0034-4885/46/8/002.
- 240 [12] Blandford R, Eichler D. Particle acceleration at astrophysical shocks: A theory of cosmic ray origin.
241 *Physics Reports* **154** (1987) 1–75. doi:10.1016/0370-1573(87)90134-7.
- 242 [13] Giacalone J. The physics of particle acceleration by collisionless shocks. *Planetary and Space Science*
243 **51** (2003) 659–664. doi:10.1016/S0032-0633(03)00101-6.
- 244 [14] Lee MA, Mewaldt RA, Giacalone J. Shock Acceleration of Ions in the Heliosphere. *Space Science*
245 *Reviews* **173** (2012) 247. doi:10.1007/s11214-012-9932-y.
- 246 [15] de Hoffmann F, Teller E. Magneto-Hydrodynamic Shocks. *Phys. Rev.* **80** (1950) 692–703. doi:10.
247 1103/PhysRev.80.692.
- 248 [16] Russell CT, Mellott MM, Smith EJ, King JH. Multiple spacecraft observations of interplanetary
249 shocks Four spacecraft determination of shock normals. *Journal of Geophysical Research* **88** (1983)
250 4739–4748. doi:10.1029/JA088iA06p04739.
- 251 [17] Dunlop MW. Four-point Cluster application of magnetic field analysis tools: The Curlometer. *Journal*
252 *of Geophysical Research* **107** (2002) 14. doi:10.1029/2001JA005088.
- 253 [18] Reme H, Bosqued JM, Sauvaud JA, Cros A, Dandouras J, Aoustin C, et al. The Cluster Ion
254 Spectrometry (cis) Experiment. *Space Sci. Rev.* **79** (1997) 303. doi:10.1023/A:1004929816409.
- 255 [19] McFadden JP, Carlson CW, Larson D, Ludlam M, Abiad R, Elliott B, et al. The THEMIS ESA Plasma
256 Instrument and In-flight Calibration. *Space Sci. Rev.* **141** (2008) 277. doi:10.1007/s11214-008-9440-2.
- 257 [20] McFadden JP, Carlson CW, Larson D, Bonnell J, Mozer F, Angelopoulos V, et al. THEMIS ESA
258 First Science Results and Performance Issues. *Space Sci. Rev.* **141** (2008) 477. doi:10.1007/
259 s11214-008-9433-1.

- 260 [21] Angelopoulos V. The THEMIS Mission. *Space Science Reviews* **141** (2008) 5–34. doi:10.1007/
261 s11214-008-9336-1.
- 262 [22] Pollock C, Moore T, Jacques A, Burch J, Gliese U, Omoto T, et al. Fast Plasma Investigation for
263 Magnetospheric Multiscale. *Space Science Reviews* **199** (2016) 331. doi:10.1007/s11214-016-0245-4.
- 264 [23] Greenstadt EW, Scarf FL, Russell CT, Formisano V, Neugebauer M. Structure of the quasi-
265 perpendicular laminar bow shock. *J. Geophys. Res.* **80** (1975) 502. doi:10.1029/JA080i004p00502.
- 266 [24] Greenstadt EW, Scarf FL, Russell CT, Gosling JT, Bame SJ, Paschmann G, et al. A macroscopic
267 profile of the typical quasi-perpendicular bow shock - Isee 1 and 2. *J. Geophys. Res.* **85** (1980)
268 2124–2130.
- 269 [25] Russell C, Hoppe M, Livesey W, Gosling J. Isee-1 and-2 observations of laminar bow shocks- velocity
270 and thickness. *Geophys. Res. Lett.* **9** (1982) 1171.
- 271 [26] Mellott MM, Greenstadt EW. The structure of oblique subcritical bow shocks - ISEE 1 and 2
272 observations. *J. Geophys. Res.* **89** (1984) 2151–2161. doi:10.1029/JA089iA04p02151.
- 273 [27] Farris M, Russell C, Thomsen M. Magnetic structure of the low beta, quasi-perpendicular shock. *J.*
274 *Geophys. Res.* **98** (1993) 15285–15294.
- 275 [28] Balikhin MA, Zhang TL, Gedalin M, Ganushkina NY, Pope SA. Venus Express observes a new
276 type of shock with pure kinematic relaxation. *Geophysical Research Letters* **35** (2008) L01103.
277 doi:10.1029/2007GL032495.
- 278 [29] Wilson III LB, Koval A, Szabo A, Stevens ML, Kasper JC, Cattell CA, et al. Revisiting the structure
279 of low-Mach number, low-beta, quasi-perpendicular shocks. *Journal of Geophysical Research (Space*
280 *Physics)* **81** (2017) 2097–9133. doi:10.1002/2017JA024352.
- 281 [30] Pope SA, Gedalin M, Balikhin MA. The First Direct Observational Confirmation of Kinematic
282 Collisionless Relaxation in Very Low Mach Number Shocks Near the Earth. *J. Geophys. Res* **165**
283 (2019) 3–15. doi:10.1029/2018JA026223.
- 284 [31] Pope SA. A Survey of Venus Shock Crossings Dominated by Kinematic Relaxation. *J. Geophys. Res*
285 **125** (2020) A028256. doi:10.1029/2020JA028256.
- 286 [32] Gedalin M, Zilbersher D. Non-diagonal ion pressure in nearly-perpendicular collisionless shocks.
287 *Geophysical Research Letters* **22** (1995) 3279–3282. doi:10.1029/95GL03284.
- 288 [33] Gedalin M. Ion reflection at the shock front revisited. *Journal of Geophysical Research* **101** (1996)
289 4871–4878. doi:10.1029/95JA03669.
- 290 [34] Gedalin M. Noncoplanar magnetic field in the collisionless shock front. *Journal of Geophysical*
291 *Research: Space Physics (1978–2012)* **101** (1996) 11153–11156. doi:10.1029/96JA00518.
- 292 [35] Newbury JA, Russell CT, Gedalin M. The determination of shock ramp width using the noncoplanar
293 magnetic field component. *Geophysical Research Letters* **24** (1997) 1975–1978. doi:10.1029/
294 97GL01977.
- 295 [36] Gedalin M. Low-frequency nonlinear stationary waves and fast shocks: Hydrodynamical description.
296 *Physics of Plasmas* **5** (1998) 127–132. doi:10.1063/1.872681.
- 297 [37] Gedalin M, Newbury JA, Russell CT. Shock profile analysis using wavelet transform. *Journal of*
298 *Geophysical Research* **103** (1998) 6503–6512. doi:10.1029/97JA03593.
- 299 [38] Anderson BJ, Acuña MH, Lohr DA, Scheifele J, Raval A, Korth H, et al. The Magnetometer Instrument
300 on MESSENGER. *Space Science Reviews* **131** (2007) 417–450. doi:10/b4gh69.
- 301 [39] Winslow RM, Anderson BJ, Johnson CL, Slavin JA, Korth H, Purucker ME, et al. Mercury’s
302 magnetopause and bow shock from MESSENGER Magnetometer observations. *J. Geophys. Res* **118**
303 (2013) 2213–2227. doi:10.1002/jgra.50237.

- 304 [40] Bale SD, Balikhin MA, Horbury TS, Krasnoselskikh VV, Kucharek H, Möbius E, et al. Quasi-
305 perpendicular Shock Structure and Processes. *Space Science Reviews* **118** (2005) 161–203. doi:10.
306 1007/s11214-005-3827-0.
- 307 [41] Krasnoselskikh V, Balikhin M, Walker SN, Schwartz S, Sundkvist D, Lobzin V, et al. The Dynamic
308 Quasiperpendicular Shock: Cluster Discoveries. *Space Science Reviews* **178** (2013) 535–598. doi:10.
309 1007/s11214-013-9972-y.
- 310 [42] Gosling JT, Thomsen MF. Specularly reflected ions, shock foot thicknesses, and shock velocity
311 determinations in space. *J. Geophys. Res* **90** (1985) 9893–9896. doi:10.1029/JA090iA10p09893.
- 312 [43] Balikhin MA, Zhang TL, Gedalin M, Ganushkina NY, Pope SA. Venus Express observes a new
313 type of shock with pure kinematic relaxation. *Geophys. Res. Lett.* **35** (2008) L01103. doi:10.1029/
314 2007GL032495.
- 315 [44] Gedalin M, Friedman Y, Balikhin M. Collisionless relaxation of downstream ion distributions in
316 low-Mach number shocks. *Phys. Plasmas* **22** (2015) 072301. doi:10.1063/1.4926452.
- 317 [45] Gedalin M. Collisionless relaxation of non-gyrotropic downstream ion distributions: dependence on
318 shock parameters. *J. Plasma Phys.* **81** (2015) 905810603. doi:10.1017/S0022377815001154.
- 319 [46] Gedalin M. Kinematic Collisionless Relaxation of Ions in Supercritical Shocks. *Frontiers in Physics* **7**
320 (2019) 692. doi:10.3389/fphy.2019.00114.
- 321 [47] Gedalin M. How non-stationary are moderately supercritical shocks? *J. Plasma Phys.* **85** (2019)
322 905850505. doi:10.1017/S0022377819000692.
- 323 [48] Gedalin M. Ion heating in oblique low-Mach number shocks. *Geophys. Res. Lett.* **24** (1997)
324 2511–2514. doi:10.1029/97GL02524.
- 325 [49] Gedalin M. Shock Heating of Directly Transmitted Ions. *ASTROPHYSICAL JOURNAL* **912** (2021)
326 82. doi:10.3847/1538-4357/abf1e2.
- 327 [50] Gedalin M. Transmitted, reflected, quasi-reflected, and multiply reflected ions in low-Mach number
328 shocks. *J. Geophys. Res* **121** (2016) 10. doi:10.1002/2016JA023395.
- 329 [51] Gedalin M, Pogorelov NV, Roytershteyn V. Boundary Conditions at the Heliospheric Termination
330 Shock with Pickup Ions. *Astrophys. J.* **916** (2021) 57. doi:10.3847/1538-4357/ac05b7.
- 331 [52] Farris MH, Russell CT. Determining the standoff distance of the bow shock: Mach number dependence
332 and use of models. *J. Geophys. Res.* **99** (1994) 17. doi:10.1029/94JA01020.
- 333 [53] King JH, Papitashvili NE. Solar wind spatial scales in and comparisons of hourly Wind and ACE
334 plasma and magnetic field data. *J. Geophys. Res.* **110** (2005) A02104. doi:10.1029/2004JA010649.